



Pore Water Pressure Analysis in Coir Mat-Reinforced Soil Incorporating Soil-Structure Interaction

M. V. Sreya¹ · B. R. Jayalekshmi¹ · Katta Venkataramana¹

Received: 30 September 2021 / Accepted: 10 January 2022 / Published online: 30 January 2022
© The Author(s), under exclusive licence to Springer Nature Switzerland AG 2022

Abstract

The proposed study investigates the effectiveness of reinforcing the soft soil by a coir mat, a natural material, to act as a seismic soil-isolation medium. A 3D finite element simulation in PLAXIS 3D software has been carried out on models of five-storey buildings resting on raft foundations in soft soil with and without the soil-isolation mechanism. This study also deals with the coir composites, coir–polyethylene and coir–rubber were proposed to increase the durability of the coir mat. The isolated soil-structure system was exposed to four different earthquake motions, such as the ground motions corresponding to the elastic design spectrum for Zone III as per the Indian standard code (IS 1893 (Part 1): 2016), the scaled Northridge earthquake (1994), El Centro earthquake (1940) and Chi-Chi earthquake (1999). A pore water pressure analysis of soil bed has been carried out to study the efficacy of these materials to reduce the excess pore water pressure generated in soil under earthquake loading. The other parameters, such as shear strain mobilized shear strength, effective stress in soil, and roof acceleration, in the building were analyzed. Isolation efficiencies of reinforcement materials to reduce the excess pore water pressure generated in soil under different earthquake motions obtained are 75–82%, 71–80% and 67–72% with coir, coir–polyethylene and coir–rubber, respectively. The resulting shear strain in soil reinforced by isolation mats is lower than that in unreinforced soil because the isolation mats strengthen the soil. Compared to the unreinforced soil, the mobilized shear strength and effective stress in the soil are increased when it is reinforced with coir and coir composites. The roof acceleration and bottom acceleration in the building got reduced by the isolation mechanism.

Keywords Finite element simulation · Soil reinforcement · Coir mat and coir composites · Soil isolation-building system · Soil-structure interaction · Pore water pressure analysis

Introduction

During an earthquake, cyclic loading causes a pore pressure increase in saturated sands, leading to liquefaction in the worst situation. A variety of methods have been developed to assess the behavior of sand under these conditions. Construction of structures on soil having high liquefaction potential is dangerous. Simplified total stress techniques

were developed in the late 1960s and early 1970s to evaluate the possibility of liquefaction in homogenous soils on a yes/no basis. Many major recent earthquakes and more recent experimental investigations [1–4] have emphasized the dangers of using surface foundations. Even light constructions should be considered in regions where earthquake-induced liquefaction is expected. A soil element is subjected to a series of random motions during seismic shaking. The resulting cyclic shear strains deform the element, causing soil particle rearrangement in granular deposits and a volume change in the soil. If the soil becomes saturated and drainage is impossible, this volume change tendency will result in changes in pore-water pressure. Pore pressures are the quantities that relate to the stress in the pores of the material. Excess pore water pressure results from un-drained behavior and is affected by stress changes due to loading or unloading, sudden hydraulic condition changes, and consolidation. Seismic

✉ M. V. Sreya
sreya.187cv011@nitk.edu.in

B. R. Jayalekshmi
brjaya@nitk.edu.in

Katta Venkataramana
katta@nitk.edu.in

¹ Department of Civil Engineering, National Institute of Technology Karnataka, Surathkal, Mangalore 575025, India

shaking also causes significant settlements, which can lead to operational and even structural failure. The progressive loss of the foundation bearing capacity is caused by excessive pore pressure build-up and the accompanying shear strength degradation of the liquefiable soil layers. In the presence of a suitably thick and shear resistant non-liquefiable soil crust between the foundation and the liquefiable subsoil, the preceding impacts become less obvious and those may even be avoided [5, 6]. However, current engineering practice lacks a generally acknowledged analytical approach that would enable performance-based surface foundation design in such soil profiles. There are several solutions available today that can address and/or mitigate some geotechnical faults to reduce settlements and enhance the strength of the soil foundation. To overcome these challenges, a variety of techniques are available, including geo-synthetic reinforcement [7–13], stage construction, excavation and replacement, using lightweight fill, pre-fabricated vertical drains [14, 15], pile reinforcement (pile-supported embankments) and others.

Concerns about the environment and waste management issues may increase interest in developing and implementing environmentally friendly products and practices. In this background, industries and researchers are searching for renewable materials to replace traditional materials produced from fossil fuels. [5, 16, 17]. The 12th Sustainable Development Goal, titled "Responsible Consumption and Production," aims to promote economic growth and sustainable development by altering consumption and production habits and improving hazardous and polluting waste disposal. Natural fibre-reinforced composites [6, 18, 19] are more prevalent in the automotive and construction industries. They are utilized in construction as low-cost housing and seismic-resistant structures. Lignocellulosic fibers are abundant in nature and readily reusable and are sometimes regarded as natural waste. They have low density, cheap cost, non-toxicity, and biodegradability, making them viable to synthetic fibers in composite production [20, 21]. These fibers, however, are burned, used as low-cost energy, improperly disposed of, or composted when considered as waste [22]. As a result, new applications for such waste products

must be developed, considering environmental and economic aspects [23]. According to data from the United Nations' Food and Agriculture Organization, coconut trees cover about 12 million hectares of total global land and produce roughly 62 million tons of coconut fruit annually, totaling around 50 billion fruits annually [24]. Therefore, the present study deals with analyzing coir products as reinforcement materials to act as isolation materials to control the seismic responses, including pore pressure generated in soil. The materials used are coir (C) mat composited with other isolation materials, such as polyethylene (PE) foam and rubber (RU) mat to form C-PE and C-RU.

Coir is a fibrous coconut cover with a length of 50–350 mm approximately, and coir contains tannin, pectin, cellulose and a high amount of lignin. As the lignin content in the coir fibre is high, it is long-lasting compared to other fibers, such as jute, sisal, etc. Coir is available in the form of fibers as well as mat in industries. Even though geo-synthetics can stabilize the soil, the coir fibre is used to do it because of various advantages; with a higher coefficient of friction between soil and coir fibre, it enhances soil reinforcement more efficiently than other reinforcement materials [25]. Basic research in the application of coir as a reinforcement material began in the 1990s. Coir fibers have been used in the soil to enhance its strength and reduce liquefaction [26, 27]. The cyclic tri-axial test conducted on uniformly graded fine sand reinforced with woven and non-woven geotextile and coir fibre concluded that the liquefaction potential is reduced significantly in the sand deposit [26]. Furthermore, the length of the reinforcement fibre is a factor to be considered since long fibers are shown to improve liquefaction resistance by reducing the interstitial pressure. Long fibers increase the number of cycles needed

Table 1 Properties of soil and isolation mats

Properties	Soil	Isolation mat		
	Sand	Coir	Polyethylene foam	Rubber
Unit weight (kN/m ³)	16	10	0.22	15
Young's modulus (kN/m ²)	65	4100	22	100
Poisson's ratio	0.4	0.3	0.1	0.49
Friction angle (Degrees)	36	46	35	35
Yield stress (kN/m ²)	0.3	30	0.3	25
Tangential modulus (kN/m ²)	30	500	5	2
Hydraulic conductivity (m/s)	5×10^{-5}	5.5×10^{-4}	1×10^{-9}	2×10^{-7}

Table 2 Properties of building and raft foundation

Properties	Unit	Value
Unit weight	kN/m ³	25
Young's modulus	kN/m ²	25×10^3
Poisson's ratio	-	0.15

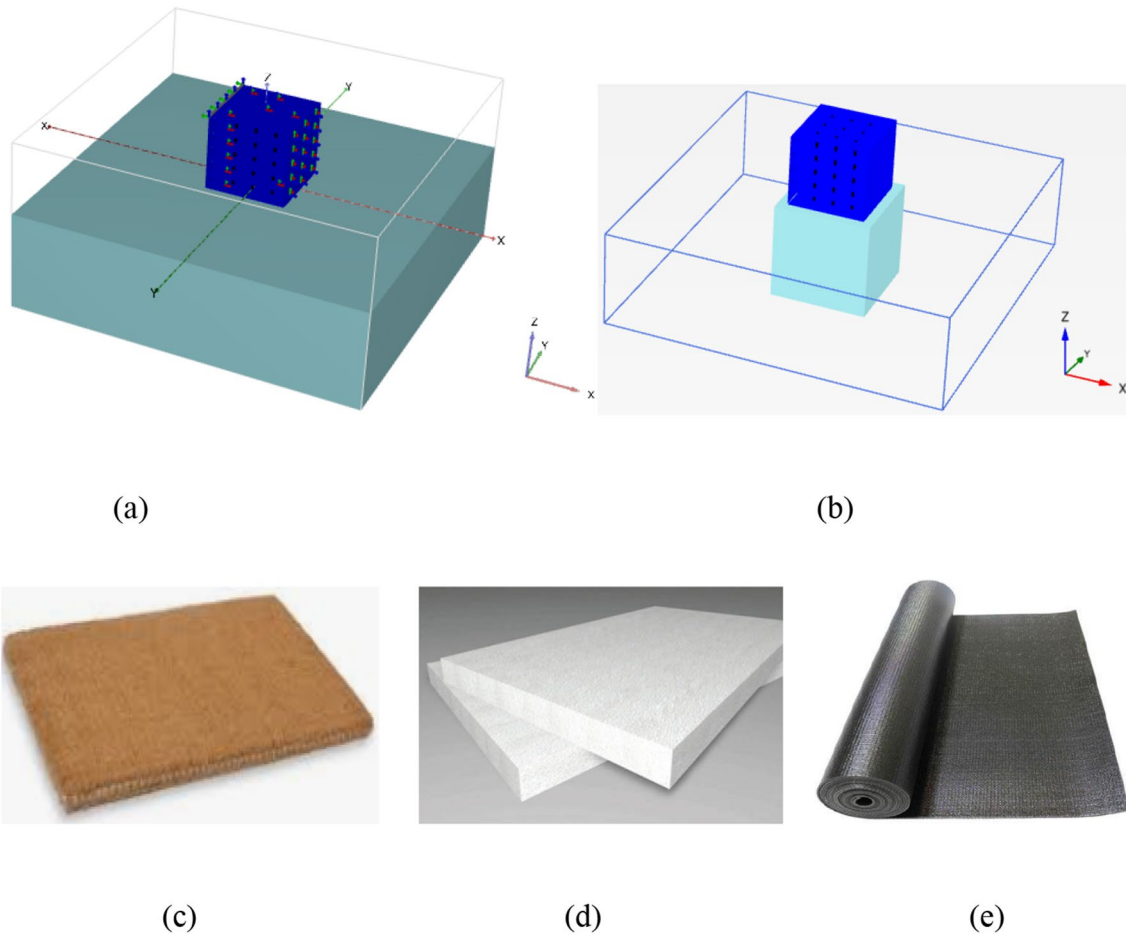


Fig. 1 Geometric model of the soil-structure system in Plaxis3D; (a) soil-structure system (b) central portion of soil covering the superstructure and Photographs of; (c) Coir mat (d) Polyethylene foam (e) Rubber mat

to achieve resistance to liquefaction. Soil strengthening with fibre inclusion could limit or prevent lateral motion due to dynamic load [27]. Shake table experiments were conducted with geo-grid, geo-synthetic fibers, and natural coir fibre reinforced in Solani sand [28] and the results were presented. The resistance to liquefaction with the soil reinforcement by the synthetic and coir fibre in the sand was improved about 88% and 91%, with 0.75% of fibre. In contrast, the strengthening by five geo-grid layers indicates an improvement of around 31% for an input motion with PGA of 0.1 g.

Coconut fibers are 4–6 times more sustainable than other fibers and are used for slope stabilization in railway embankments, waterway protection, rural unpaved road reinforcement, sub-basis layer on highways, land reclamation, and filtration in road drains [29]. The durability of coir fibre can be increased by coating the fibers with bitumen and phenol [28]. Chemical treatment is the most common method for increasing the longevity and mechanical properties of natural fibers. Coconut fibre was chemically treated with silane, alkaline, and silane alkalized coconut

fibre at various concentrations [30]. Polyethylene foam and rubber materials serve as effective isolation materials [31–34]. As a result, the current study employs rubber and polyethylene foam as coir composite materials to serve efficient seismic isolation and durability to coir mat. Because of the porosity and rubber content, research on the compressive strength of tyre shreds [33] revealed that it was very compressible. Rubber has also been used as isolation mats beneath railway embankment ballast [35]. The rubber-stabilized (reinforced with a rubber mat), highly rigid substratum ballast was shown to significantly reduce ballast settlement and degradation. It was discovered that, due to its high damping efficiency, the rubber

mat would absorb a significant amount of vibration energy, thereby protecting the structure above it. Polyethylene foam is a synthetic, high-quality material that absorbs vibration energy while also protecting the structure. It is made up of extremely long chains of ethylene, which all align in the same direction. It derives its strength largely from the length of each molecule (chain). The extremely long polymer chains enable load transfer by strengthening intermolecular interactions. Polyethylene fibers are manufactured in a gel spinning process. The high molecular weight is what gives polyethylene a unique combination of high impact strength, low coefficient of friction, and abrasion resistance. Polyethylene foams do not leach and are

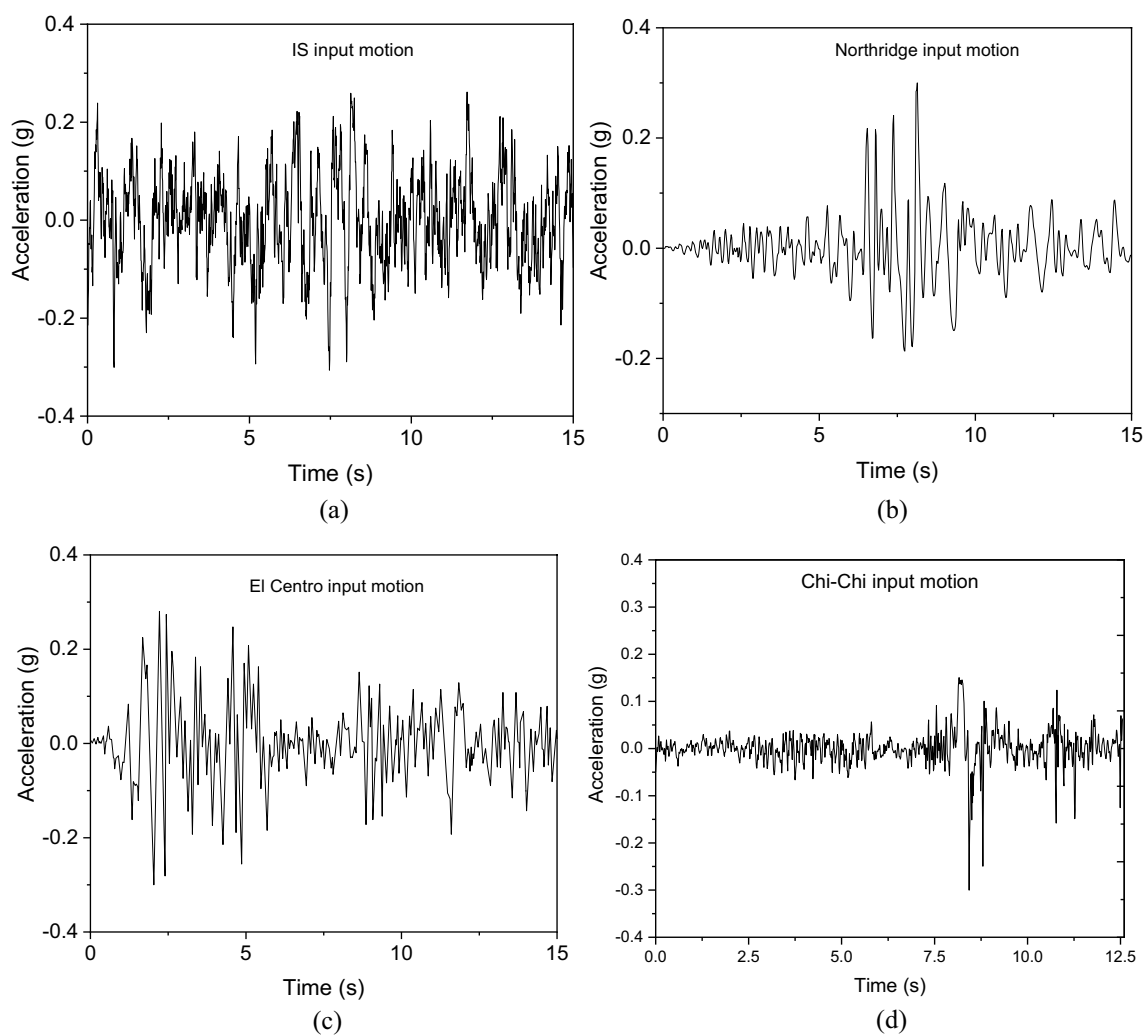


Fig. 2 Input acceleration time history of the actual earthquake input motions (a) IS (b) El Centro (c) Northridge (d) Chichi

not affected by chemical or biological degradation [36]. The inclusion of waste high-density polymer foam strips in soil with appropriate amounts dramatically increased the shear strength and sand ductility [37, 38]. This studies on the use of these reinforcement materials mainly in the form of fibers and strips are described in the literature. Since the length of fibre helps in increasing the isolation efficiency of the reinforcement materials, the current study proposes the modelling of reinforcing materials in their mat form for soil-isolation purposes. From the literature survey, it is observed that polyethylene foam and rubber are durable materials used to strengthen soil behind the retaining wall, slope stabilization, etc. [31, 34, 39]. The application of these materials to support the shallow foundation for the structures and its suitability as vibration absorbers has to be examined yet. It is also observed from the previous studies that there are no studies existing on the use of coir mat and its composite mats as the isolation material in soil for isolating pore water pressure in soil. The possibility of using low to high dense and stiff material is of great importance to study its effectiveness to act as isolation materials. The numerical modelling of these materials can be done in PLAXIS software since it provides a number of advantages such as ability to deal with excess pore pressure phenomena, estimate the excess pore pressure during plastic calculations in un-drained soil and easy to understand soil-structure interaction. The software can also replicate the constitutive soil models for modeling non-linear behavior.

This study aims to create a 3D finite element (FE) numerical model for simulating the performance of an isolation mat-reinforced soil structure system under different earthquake loading conditions. The soil-structure system is modelled in finite element based PLAXIS 3D software. The proposed study analyzes the isolation efficiency of the coir mat and its composites under different input motions. The soil-structure responses, such as acceleration of building,

excess pore water pressure in the soil, shear strain mobilized shear strength and effective stress of soil, are examined. The results obtained from the reinforced and unreinforced soil are compared, and the influence of isolation materials in reducing the seismic responses in soil-structure system is evaluated. Combining the coir mat with other isolation mats is the novel technique introduced in the study; the compositing material increases both isolation efficiency as well as durability of the coir mat.

Methodology

The numerical simulation is intended to be carried out using the finite element method since it enables modeling complicated nonlinear soil behavior and different interface conditions with varying geometries and soil characteristics. PLAXIS 3D 2016 was selected for the numerical analysis of this work to simulate the three-dimensional behavior of the soil-structure system. Axisymmetric modeling is appropriate for this analysis. The soil in the FE model was represented using the built-in 10-node tetrahedral elements which incorporate the stress-strain behavior. This element type offers second-order displacement interpolation.

Furthermore, it retains the geometry preferred in 3D mesh creation. The hardening soil model is used to simulate the soil bed, which requires modulus properties and strength variables, such as angle of shearing resistance and cohesion. Input parameters of soil used are shown in Table 1. In order to demonstrate the correct load distribution and deflection patterns, the soil bed was extended 3.5 times raft width laterally and 1.5 times raft width downwards. An isolation mat was placed at the foundation and soil interface to function as absorbers and relieve the vibration energy transfer to the structure. Isolation mats are also modeled using the hardening soil model. Isolation mats are provided for a dimension of 20m × 20m × 0.5 m which covers the bottom area of the raft foundation with 1 m extensions in all four directions at 1 m below the raft foundation. Coir composites were modeled with each layer of composite materials having a thickness of 0.5 m provided at top and bottom sandwiched with 0.5 m of coir mat in the middle to get an adequate total thickness of 1.5 m. The bottom of the geometry is fixed, while upward movement is permitted. The plate element is used to model the building frames.

The building frames are made up of concrete. The modulus of elastic (E) for concrete was calculated according to the grade of concrete as per IS-456 2000 ($E = 5000$

Table 3 Fourier amplitude and specific energy density corresponding to the natural frequency of the reinforced soil-structure system

Earthquake	Fourier amplitude Soft soil	Specific energy density (m^2/s)
Indian Standard (EQ-1)	0.252	0.4726
Northridge (EQ-2)	0.219	0.2110
El Centro (EQ-3)	0.11642	0.1805
Chi-chi (EQ-4)	0.0657	0.0522

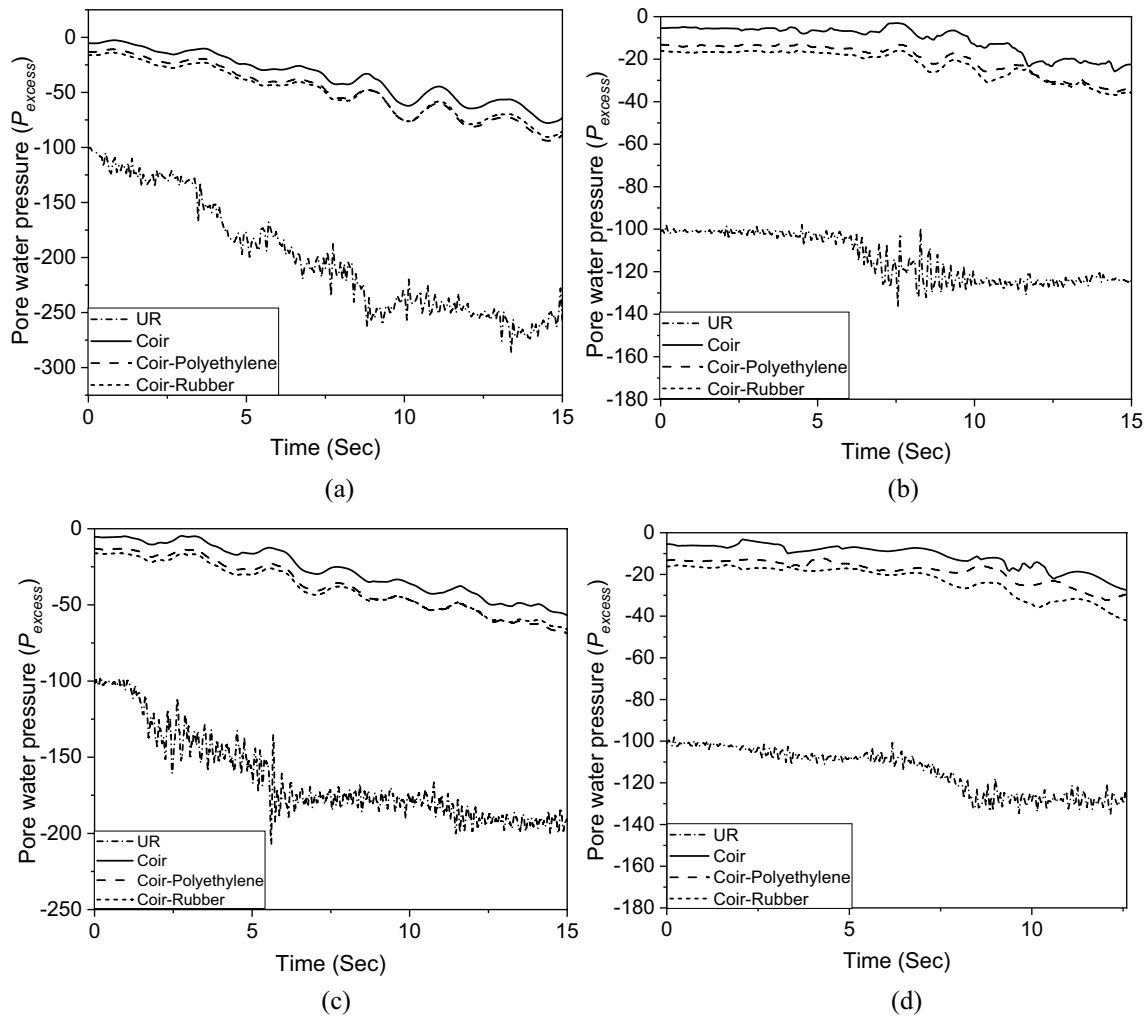
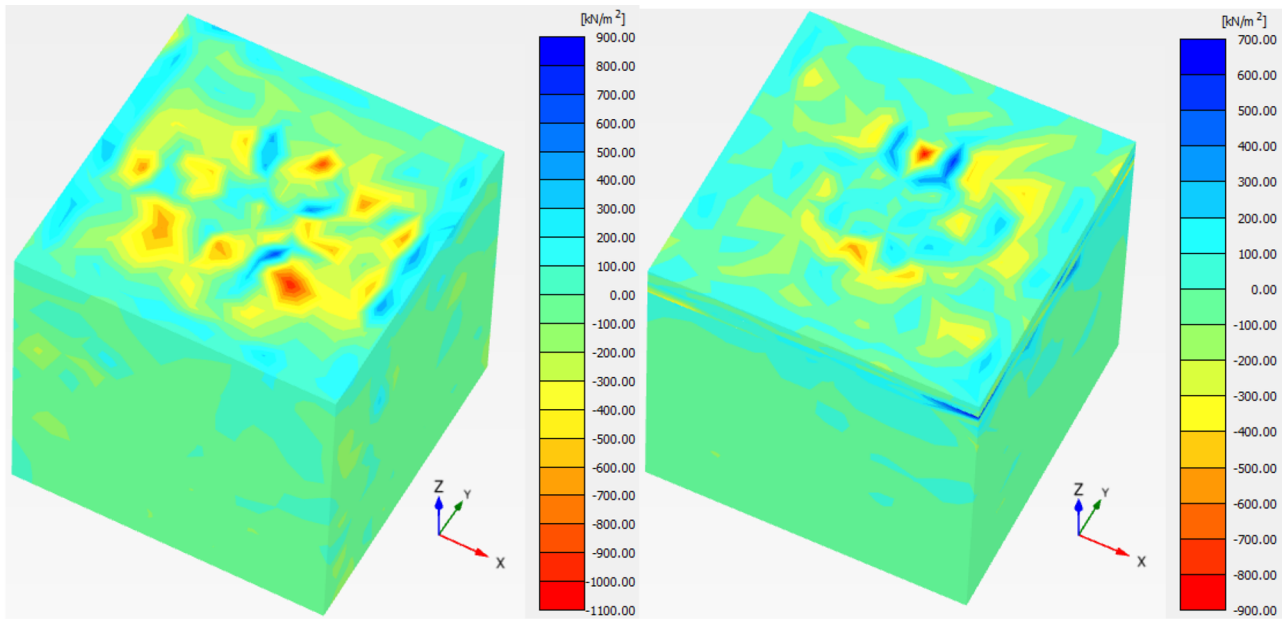


Fig. 3 Excess pore water pressure–time history in soil for reinforced and unreinforced cases under different earthquake input motions; (a) EQ-1, (b) EQ-2, (c) EQ-3, (d) EQ-4

$\sqrt{f_{ck}}$), where f_{ck} is the characteristic compressive strength of concrete. The modulus and stiffness characteristics of a plate are shown in Table 2. Only the influence of gravity loads of the supporting soil and building frames and reinforcement materials are considered in the static analysis of the soil-structure system. The geometry of a soil-structure system is illustrated in Fig. 1. The Fig. 1 also shows the photographs of isolation mats. The first phase in the study was to create the mesh and determine the initial stress at rest, followed by the plastic analysis and dynamic analysis.

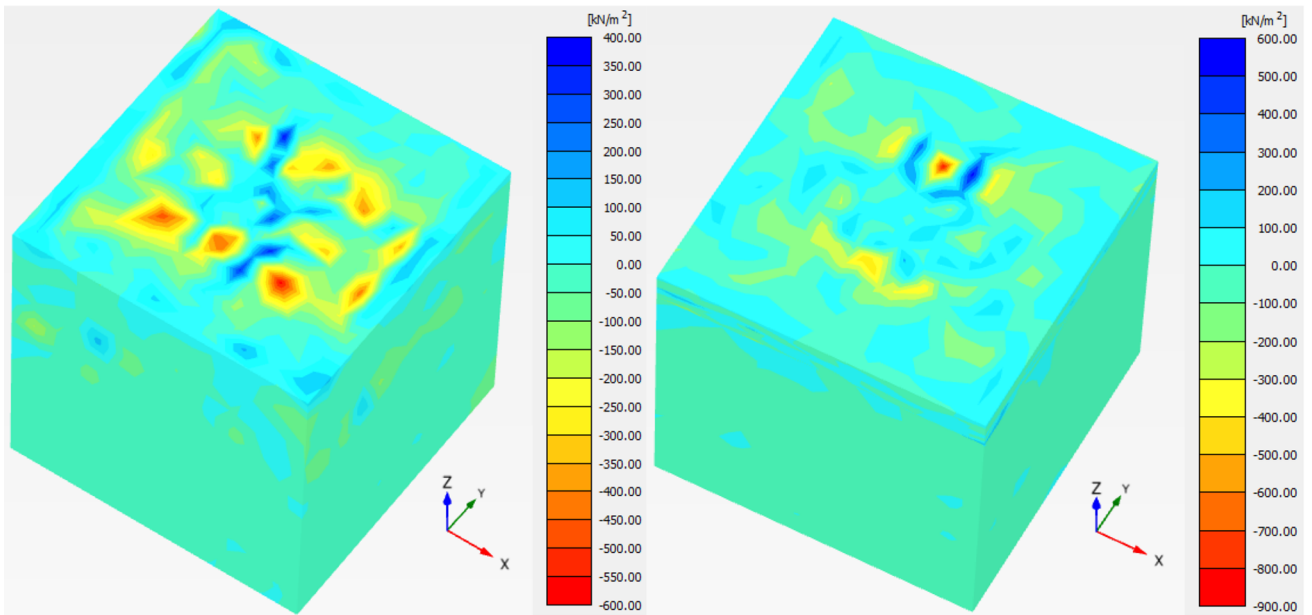
Hardening soil model (HS model)

The hardening soil model is an advanced hyperbolic soil model. The stiffness approach is the primary difference of the hardening soil model with the Mohr–Coulomb model. Here, the soil is represented considerably more accurately by incorporating three distinct input stiffness: tri-axial loading stiffness E_{50} , tri-axial unloading stiffness E_{ur} and the oedometer loading stiffness E_{oed} . Apart from that, it allows for stress-dependency of the stiffness moduli. The hardening



(a) Unreinforced soil

(b) Reinforced soil



(c) Unreinforced soil

(d) Reinforced soil

Fig. 4 Excess pore water pressure distribution in the soil at its central portion covering the superstructure for coir mat reinforced and unreinforced cases of soil excited under; (a)–(b) EQ-1 (c)–(d) EQ-2 (e)–(f) EQ-3 (g)–(h) EQ-4

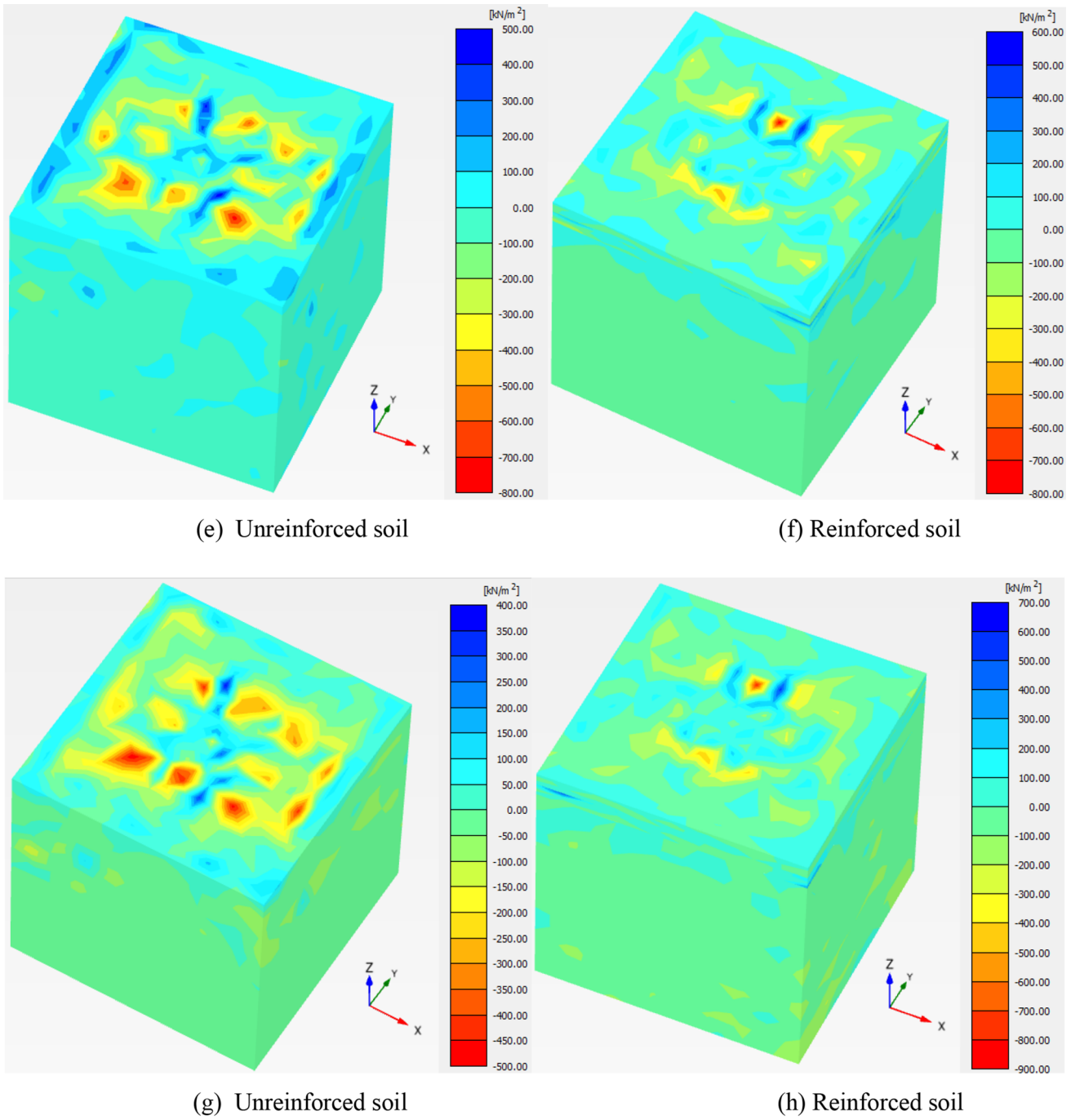


Fig. 4 (continued)

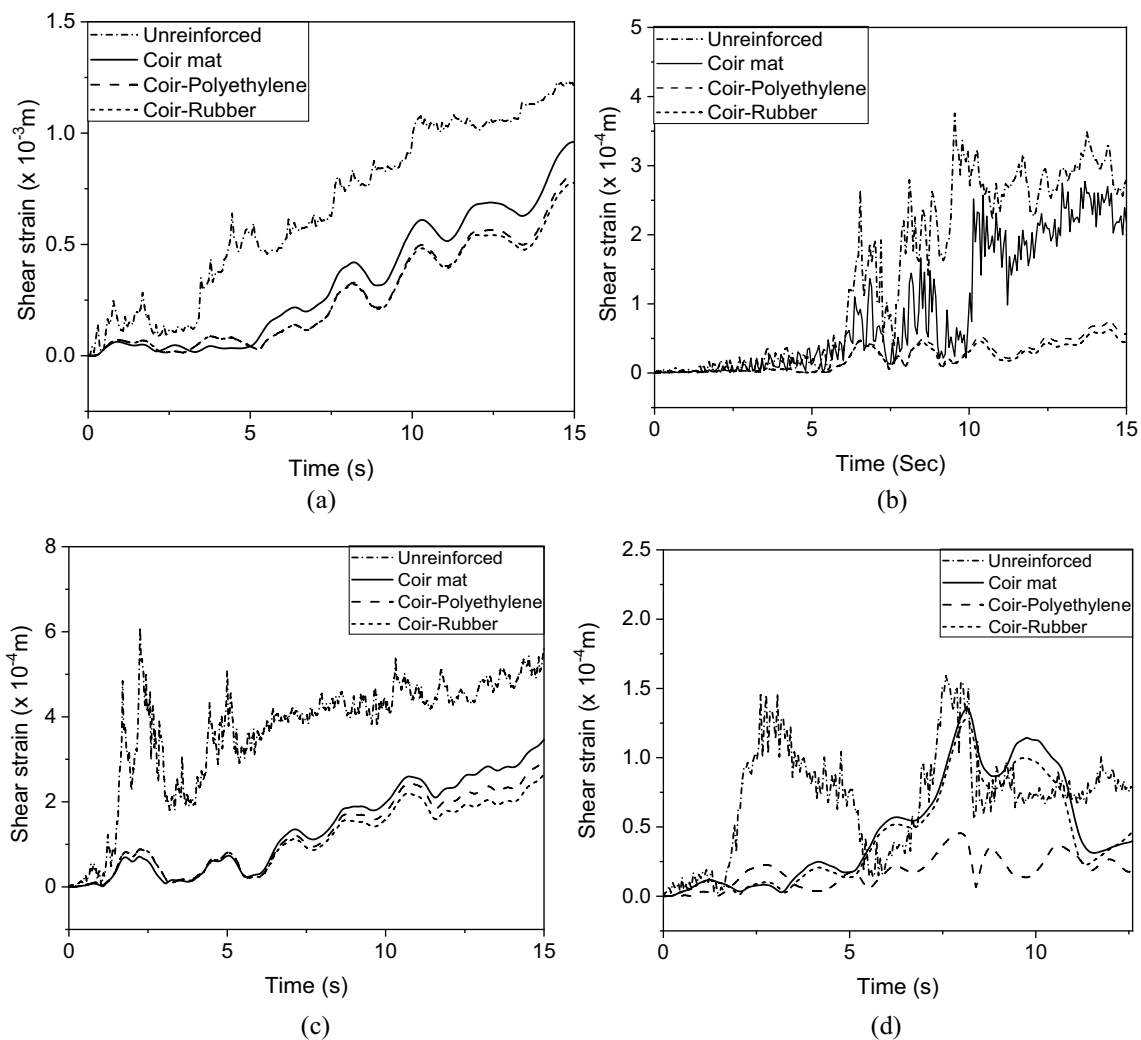
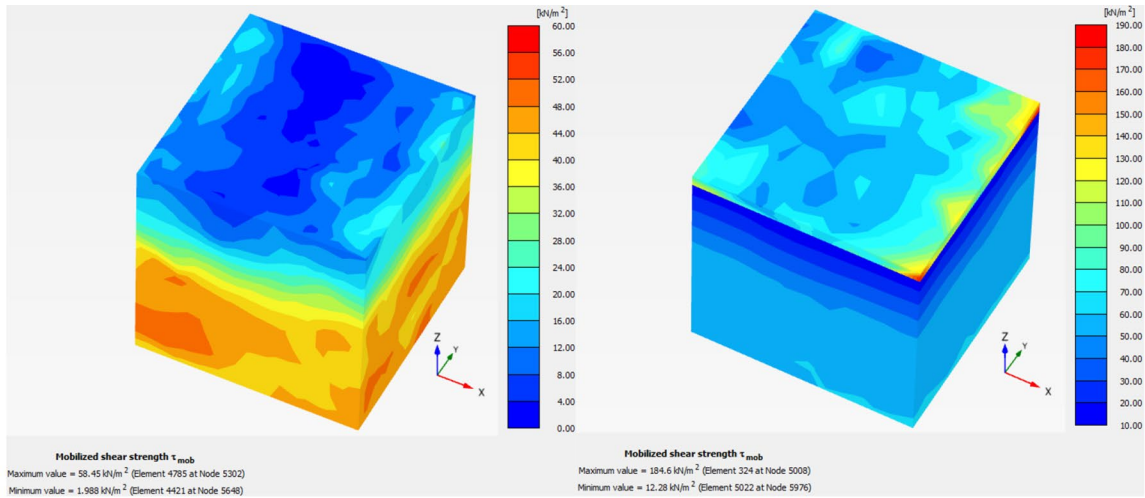


Fig. 5 Shear strain time history in the soil for reinforced and unreinforced cases under different earthquake input motions; (a) EQ-1, (b) EQ-2, (c) EQ-3, (d) EQ-4

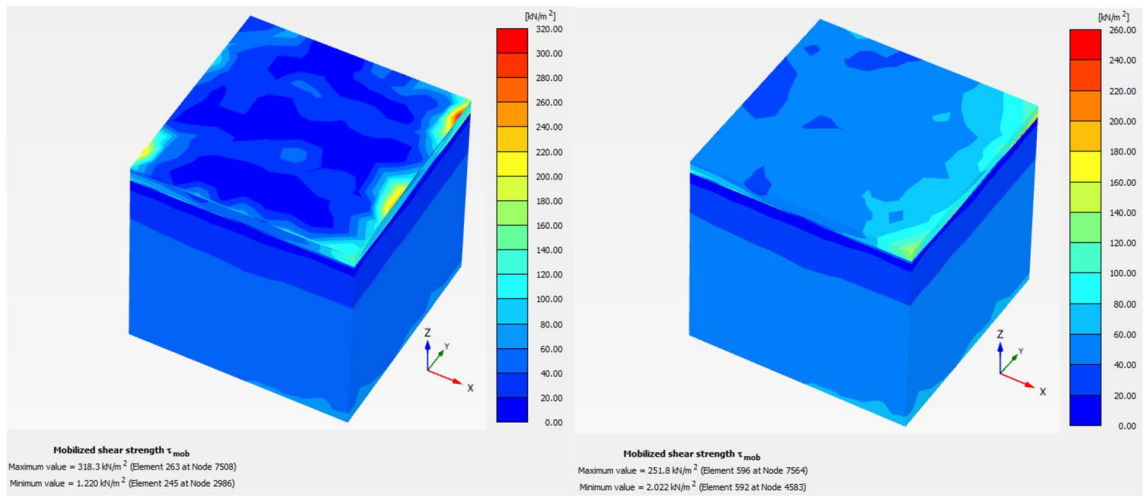
soil model is developed in the context of the classical theory of plasticity. Total strain is estimated in this model utilizing a stress-dependent stiffness that differs for virgin loading and un/re-loading. Plastic strains are determined by using multi-surface yield criteria. Hardening is considered to be

isotropic in respect of both plastic shear and volume strain. A non-related flow rule is assumed for frictional hardening, while an associated flow rule is assumed for cap hardening. The finite element (FE) analysis is utilized in this article for the soil-structure system. The PLAXIS 3D finite element



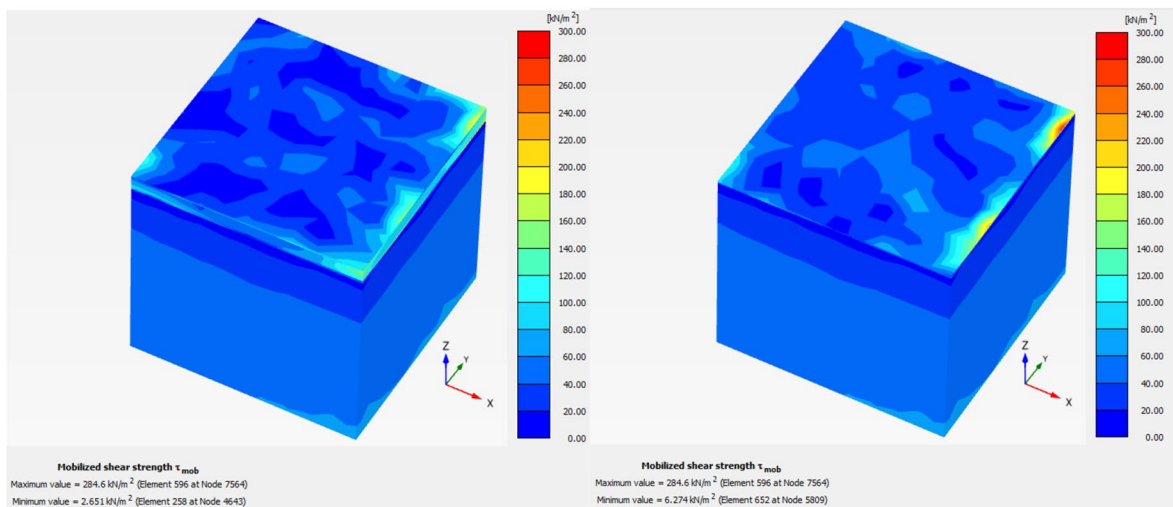
(a)

(b)



(c)

(d)



(e)

(f)

Fig. 6 Mobilized shear strength in the soil at its central portion covering the superstructure excited under EQ-1 input motion for; (a) Unreinforced soil (b) soil reinforced by coir mat (c) soil reinforced by coir–polyethylene composite (at top coir–polyethylene interface) (d) soil reinforced by coir–polyethylene composite (at bottom coir–polyethylene interface) (e) soil reinforced by coir–rubber composite (at top coir–rubber interface) (f) soil reinforced by coir–rubber composite (at bottom coir–rubber interface)

program (version 8) is used to achieve this goal. Tables 1 and 2 provide the soil and reinforcement characteristics for two distinct Mohr–Coulomb and Hard soil models [40–48].

The Calculation of Pore Water Pressure

Total stresses (σ) are the sum of effective stresses (σ') and active pore pressures (P_{active})

$$\sigma = \sigma' + P_{\text{active}} \quad (1)$$

The active pore pressure is calculated by multiplying the effective saturation (S_{eff}) by the pore water pressure (P_w).

$$P_{\text{active}} = S_{\text{eff}} \cdot P_w \quad (2)$$

When the degree of saturation is less than unity, which is usually the case when the water level rises above the phreatic level, pore water pressure differs from active pressure. P_{active} and P_w are generally equal when the water level is below the phreatic level.

As an alternative to the pore water pressure (P_w), the groundwater head (h) can be viewed as:

$$h = z - P_w / \gamma_w \quad (3)$$

where z is the vertical coordinate and γ_w is the unit weight of water. In the pore water pressure, a further distinction is made between steady-state pore pressure (P_{steady}) and excess pore pressure (P_{excess}).

$$P_w = P_{\text{steady}} + P_{\text{excess}} \quad (4)$$

where, steady-state pore pressure is the steady-state or long-term part of pore pressure.

Excess pore pressure is the result of undrained behavior and is affected by stress changes due to loading or unloading, a sudden change in hydraulic conditions and consolidation.

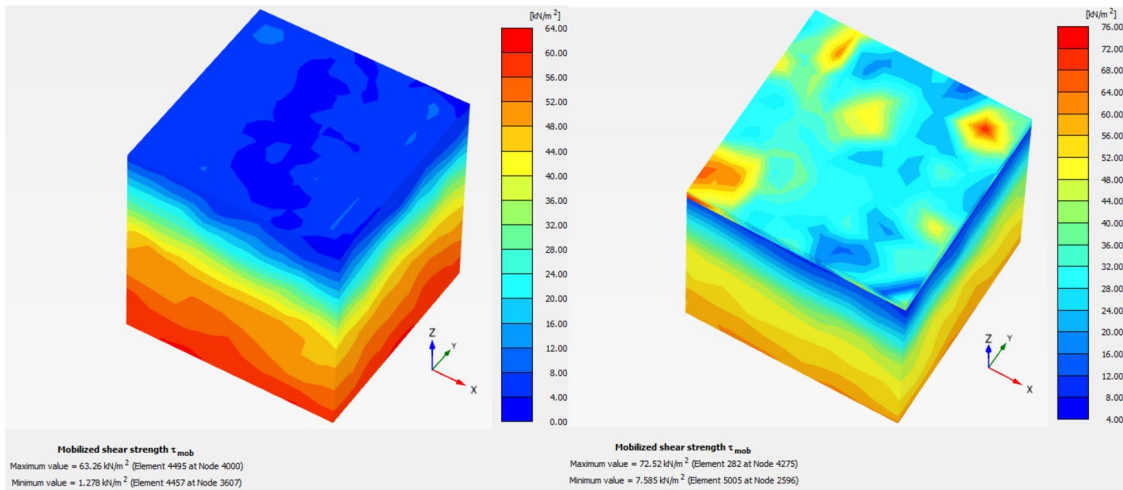
Seismic Analysis of Soil-Structure System

Soil and structures are frequently exposed to both static and dynamic stresses. If the loads are strong enough, they can cause significant damage to soil and superstructures during earthquakes. The dynamic analysis allows investigating the impacts of vibrations in the soil. A prescribed displacement at the bottom boundary is used to simulate the earthquake. To absorb outgoing waves, absorbent boundary conditions are imposed at the distant vertical limits. The typical absorbent boundaries for models are created at the left-hand, right-hand, and bottom borders. While analyzing, the absorbent borders reduce the box effect. Figure 2 depicts an actual accelerogram of an earthquake in standard SMC format (Strong Motion CD-ROM) that is used for the input motion and it is applied as a horizontal prescribed displacement to the bottom boundary. The peak ground acceleration in the accelerograms is 0.3 g. Table 3 shows the Fourier amplitude and specific energy density corresponding to the natural frequency of the reinforced soil-structure system. The seismic study is done in two stages: first with the plastic analysis, followed by dynamic analysis. The dynamic analysis time interval is 15 s.

Results and Discussion

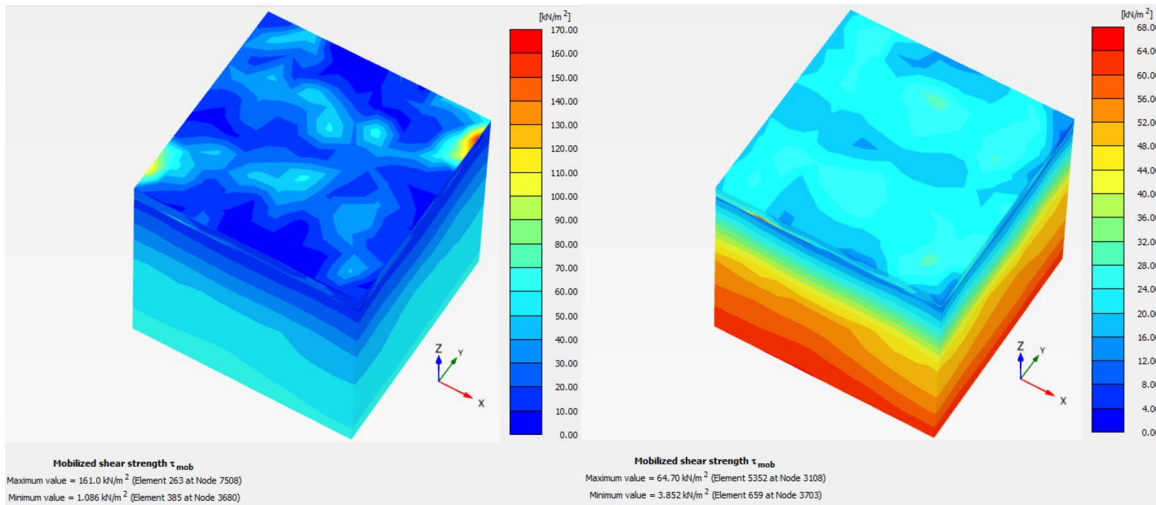
Excess Pore Water Pressure in Soil (P_{excess})

The soil in which significant pore water pressure is generated on a change in load is the most likely to liquefy. Excess pore water pressure in soil for both reinforced and unreinforced cases of soil is analyzed for different input motions. P_{excess} is noted beneath the raft foundation for unreinforced and reinforced soil. With the increase in time, pore pressure is observed to be increased for all reinforced cases of models. The reduction in P_{excess}



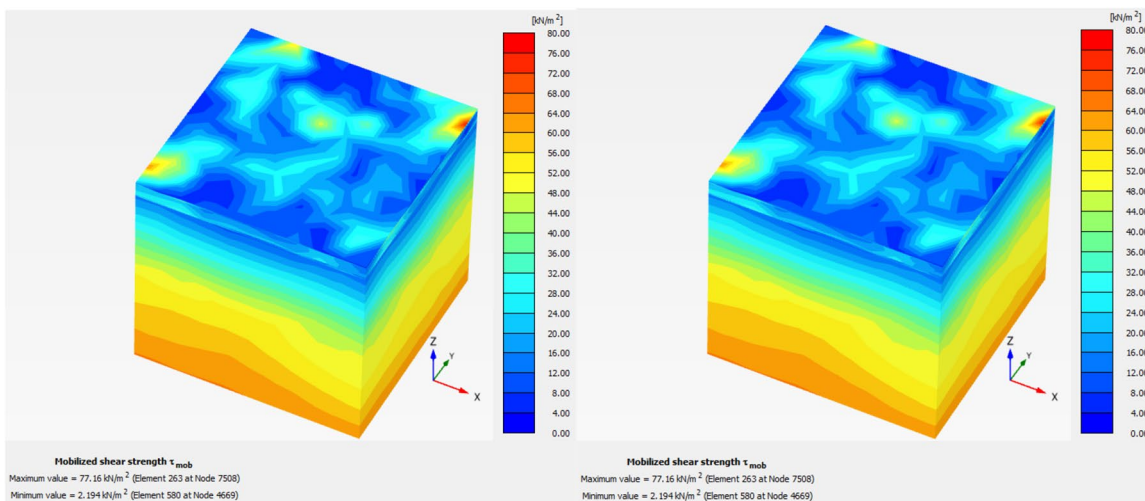
(a)

(b)



(c)

(d)



(e)

(f)

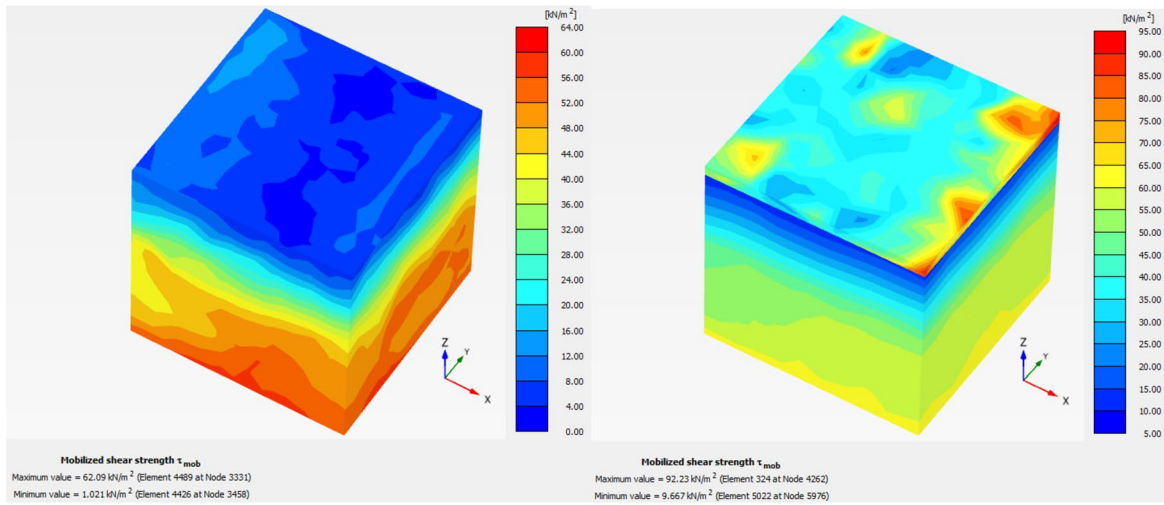
Fig. 7 Mobilized shear strength in the soil at its central portion covering the superstructure excited under EQ-2 input motion for; (a) Unreinforced soil (b) soil reinforced by coir mat (c) soil reinforced by coir–polyethylene composite (at top coir–polyethylene interface) (d) soil reinforced by coir–polyethylene composite (at bottom coir–polyethylene interface) (e) soil reinforced by coir–rubber composite (at top coir–rubber interface) (f) soil reinforced by coir–rubber composite (at bottom coir–rubber interface)

in soil under EQ-1, EQ-2, EQ-3 and EQ-4 earthquake motions obtained by the reinforcement of C mat is 76%, 75%, 82% and 81.5%, respectively, by the reinforcement of C-PE mat is 72%, 71%, 77% and 79.3% respectively and by the reinforcement of C-RU mat is 67%, 70%, 72% & 72% respectively (Fig. 3). Among the isolation mats reinforced in soil, the coir mat reduces the P_{excess} in soil considerably. Because there is a chance for water to flow through the entire length of the coir mat when the coir mat is solely placed in the soil. So that coir mat absorbs the water through its entire surfaces and reduces the further flow to the topsoil, near to the foundation. But when the C-PE and C-RU mats are implemented in the soil, the impermeable materials, such as polyethylene foam and rubber mat, will not absorb the water; therefore, there will be a chance for water to pass through the sidewise of isolation material to reach the foundation level. It is observed from the results that there is no much change in pore water pressure generated in soil when it is reinforced with C, C-PE and C-RU mats. Since coir is a natural material, there is a chance of degradation in the material as time goes. Therefore, the provision of coir–polyethylene and coir–rubber composite mats is recommended from this study. And especially coir–polyethylene shows much more isolation efficiency in reducing the P_{excess} compared to coir–rubber. The change in P_{excess} with the increase in depth of soil below the foundation is also analyzed. Figure 3 shows the excess pore water pressure–time history in soil for reinforced and unreinforced cases under different earthquake input motions. The excess pore water pressure distribution in the soil at its central portion covering the superstructure for reinforced and unreinforced cases of soil is also analyzed and shown in Fig. 4. It is clear from the contour plot that the intensity of pore water

pressure is reduced at the soil–foundation interface when the coir reinforcement is done in the soil.

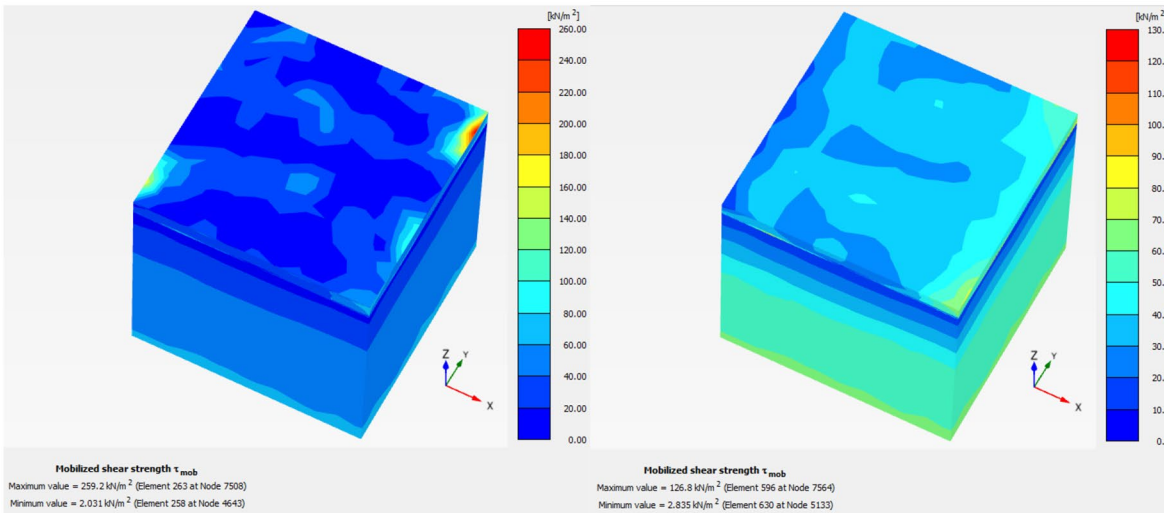
The Shear Strain and Mobilized Shear Strength of Soil

The increase in seismic-induced soil shear strain and reduction in shear strength is frequently a major concern for the overall stability of structures. With the reinforcement of isolation mats in the soil, the shear strain of soil decreases by the increase in the mobilized shear strength. The shear strain and shear strength of soil beneath the foundation are analyzed for different models under various earthquake motions. Reinforcement reduces the shear strain in the soil since the isolation materials modify the shear strength of the soil. Dynamic analysis is performed on the soil–structure system for soil without reinforcement and soil with C, C-PE and C-RU mats placed horizontally below the raft foundation. Figure 5 shows shear strain in reinforced and unreinforced soil. With the increase in the duration of earthquake motion, shear strain in the soil also increases. Shear strain reduced for soil reinforced by isolation mats. The reduction in shear strain in soil under EQ-1, EQ-2, EQ-3 and EQ-4 earthquake motions obtained by the reinforcement of C mat is 5%, 26.13%, 43.4% and 16% respectively, by the reinforcement of C-PE mat is 19%, 81%, 51% and 72% respectively and by the reinforcement of C-RU mat is 21.46%, 83.1%, 57% and 20% respectively (Fig. 5). This is because the isolation mats act as the reinforcement layer in the soil, strengthening the soil and reducing the shear strain by increasing its shear strength. The change in mobilized shear strength in reinforced soil compared to the unreinforced soil under different input motions is shown by the contour diagram in Figs. 6, 7, 8, 9. C-RU material does not show a proportionate shear strain development in soil under different input motions. Under EQ-4 input motion, shear strain developed in soil by the reinforcement of C-RU material is found to be higher than C-PE material. But under all other input motions, C-PE performs better over C-RU in the shear strain reduction in soil. The natural frequency of the soil–structure system reinforced with C-RU mat is not abundant in EQ-4 input motion. Therefore, chances of the natural frequency



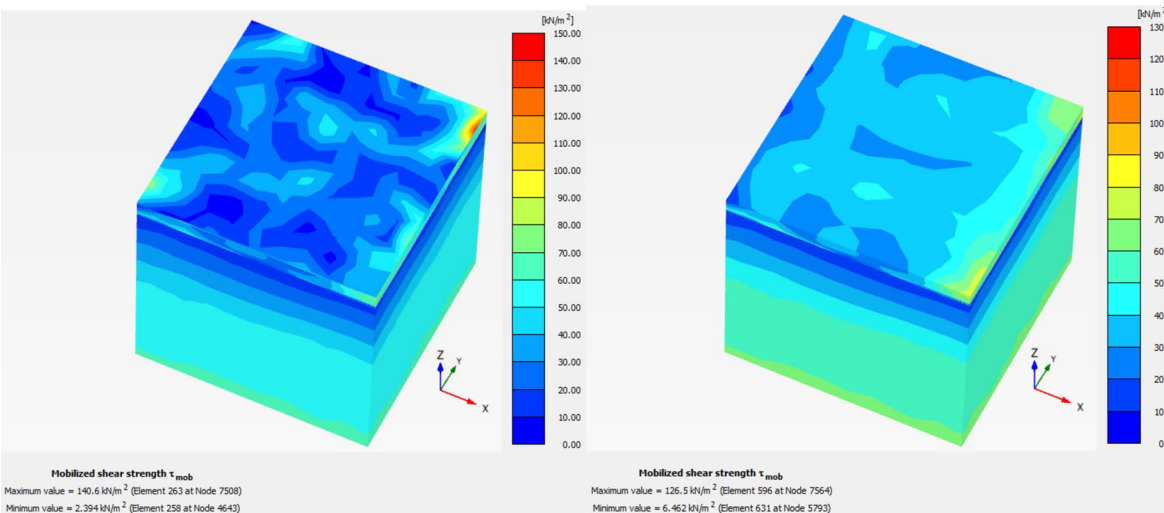
(a)

(b)



(c)

(d)



(e)

(f)

Fig. 8 Mobilized shear strength in the soil at its central portion covering the superstructure excited under EQ-3 input motion for; (a) Unreinforced soil (b) soil reinforced by coir mat (c) soil reinforced by coir–polyethylene composite (at top coir–polyethylene interface) (d) soil reinforced by coir–polyethylene composite (at bottom coir–polyethylene interface) (e) soil reinforced by coir–rubber composite (at top coir–rubber interface) (f) soil reinforced by coir–rubber composite (at bottom coir–rubber interface)

of C-RU material to match with the EQ-4 input motion are rare and so the complete efficiency of material to reduce the shear strain in soil could not be attained.

Effective Confining Stress

The inclusion of a basal reinforcement mat adds confining stress to the reinforced soil system and foundation. This increases the bearing capacity in traditional soft foundation soils while reducing the plastic failure zone, resulting in a more stable platform. Coir mat considerably improved the effective stress in soil (Fig. 10). The effective stress is observed to be decreasing with the increase in the duration of earthquakes for unreinforced soil cases. But, for reinforced soil, effective confining stress increases with the time of the earthquake and becomes constant after a particular time (Fig. 10). An increase in effective stress makes the supporting soil strong, so that liquefaction reduces in soil. In a previous study, it was observed that the stress of the fibre-reinforced soil increased rapidly as the load increased, and the confining pressure had a significant effect on the strength of the fibre-reinforced soil [49]. That is, the greater the confining pressure, the greater the reinforcement effect.

Maximum Acceleration in Building

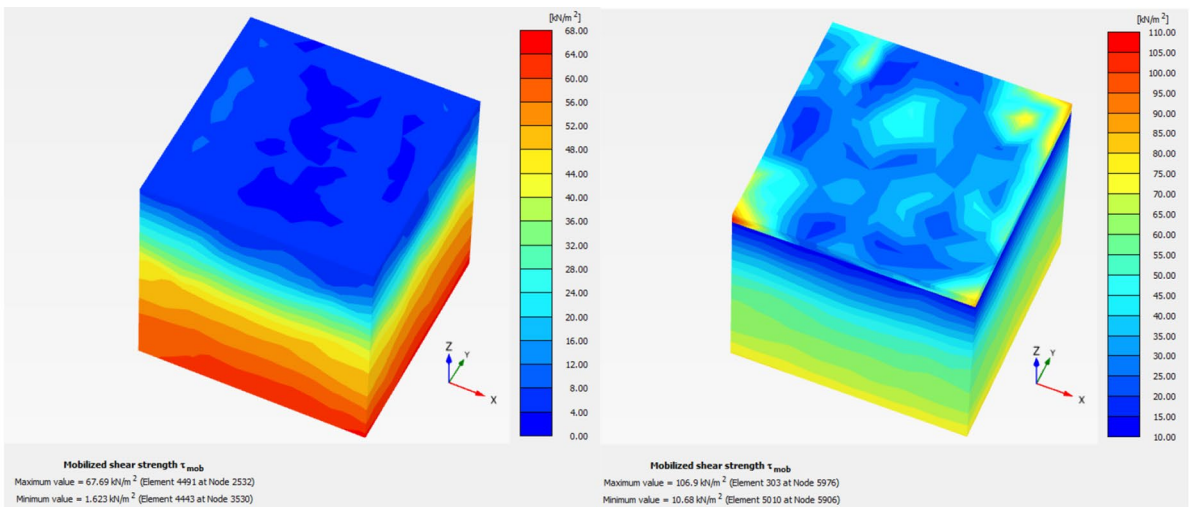
According to Fig. 11, the maximum input horizontal acceleration of 0.3 g results in an acceleration amplification in soil. The horizontal acceleration at the top and bottom of the building is analyzed for reinforced and unreinforced building cases. Soil-structure system subjected to EQ-1 earthquake motion shows higher responses for the unreinforced case

of building. All isolation mats show almost equal isolation efficiency in reducing the acceleration response in the building. The reduction in roof acceleration and bottom acceleration in building for EQ-1, EQ-2, EQ-3 and EQ-4 earthquake motions respectively obtained as 62%, 51%, 53%, 62%; 54%, 48.5%, 47.23%, 33% (Figs. 11 & 12). Coir mat and coir composites significantly reduce the acceleration in the building.

Conclusion

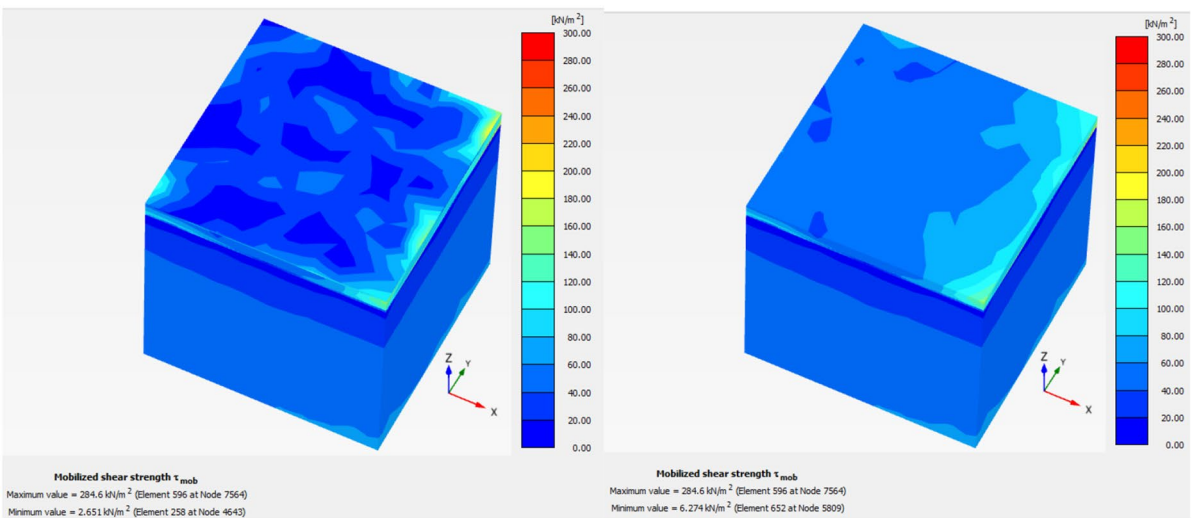
Conclusions regarding the liquefaction triggering conditions under reinforced and unreinforced soil cases drawn based on the numerical study done on the soil-structure system in PLAXIS 3D software are:

- The isolation efficiencies of reinforcement materials, C, C-PE and C-RU mats to reduce the excess pore water pressure under different earthquake motions obtained are 75–82%, 71–80%, and 67–72% respectively. Coir–polyethylene shows much more isolation efficiency in reducing the P_{excess} compared to coir–rubber. The P_{excess} increased with the increase in depth of soil below the foundation.
- The resulting shear strain for soil reinforced by isolation mats is lower than that obtained from unreinforced soil since the isolation mats strengthen the soil. The shear strength and effective stress of the soil reinforced with coir and coir composites are improved compared to the unreinforced soil.
- The reduction in roof acceleration and bottom acceleration of building resting on soil reinforced with coir mat excited under EQ-1, EQ-2, EQ-3 and EQ-4 earthquake motions respectively obtained as 62%, 51%, 53%, 62%; 54%, 48.5%, 47.23%, 33%.
- Seismic responses, such as excess pore water pressure, shear strain, shear strength and effective stress in soil and roof acceleration in building, observed to be increased with an increase in specific energy density of earthquake motion considered (Table 3). But



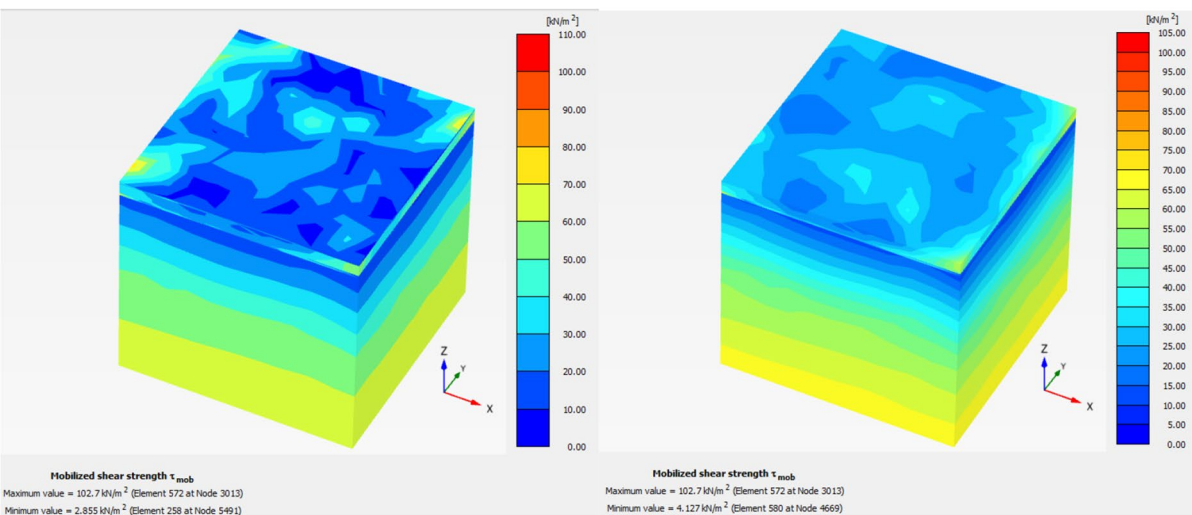
(a)

(b)



(c)

(d)



(e)

(f)

Fig. 9 Mobilized shear strength in the soil at its central portion covering the superstructure excited under EQ-4 input motion for; (a) Unreinforced soil (b) soil reinforced by coir mat (c) soil reinforced by coir–polyethylene composite (at top coir–polyethylene interface) (d) soil reinforced by coir–polyethylene composite (at bottom coir–polyethylene interface) (e) soil reinforced by coir–rubber composite (at top coir–rubber interface) (f) soil reinforced by coir–rubber composite (at bottom coir–rubber interface)

as a conflict to this conclusion, the seismic responses under El Centro input motion (specific energy density = 0.18m²/s) show higher seismic responses than that under Northridge earthquake motion (specific energy density = 0.211m²/s). This may be happened

because of the abundant frequency content available in the El Centro earthquake data which match with the natural frequency of EPS-reinforced soil-structure system.

- The dynamic analysis on coir and coir composites reinforced soil-structure system concludes that providing coir in the soil is a natural, economical and efficient isolation technique to control the liquefaction tendency of soft soil. Providing the composites of coir shows lesser efficiency in reducing the pore water pressure in the soil. Even though the composites are efficient than coir mat alone to gain the shear strength and reducing the shear strain in soil. Isolation efficiency of the polyethylene and

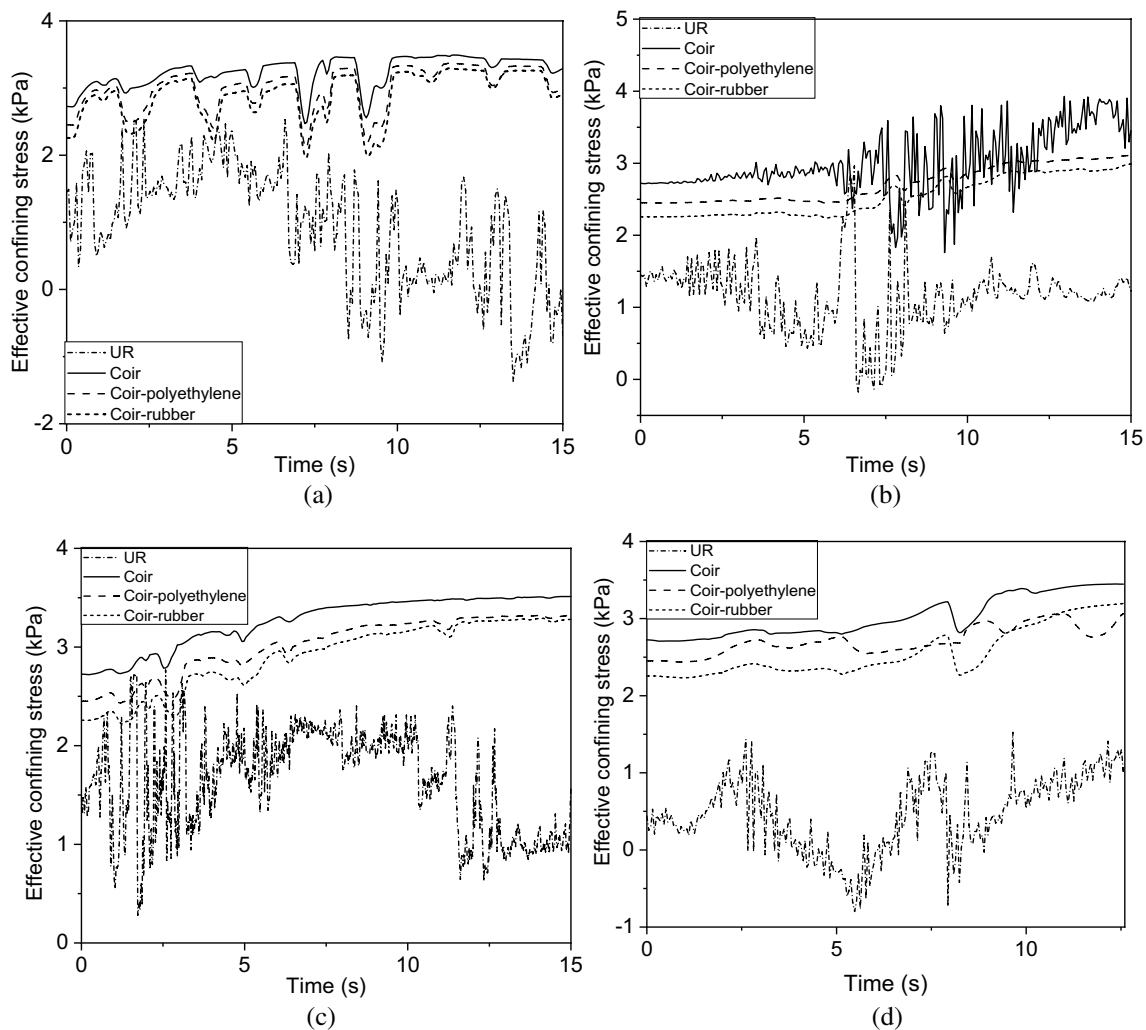


Fig. 10 Effective confining stress time history in the soil for reinforced and unreinforced cases under different earthquake input motions; (a) EQ-1, (b) EQ-2, (c) EQ-3, (d) EQ-4

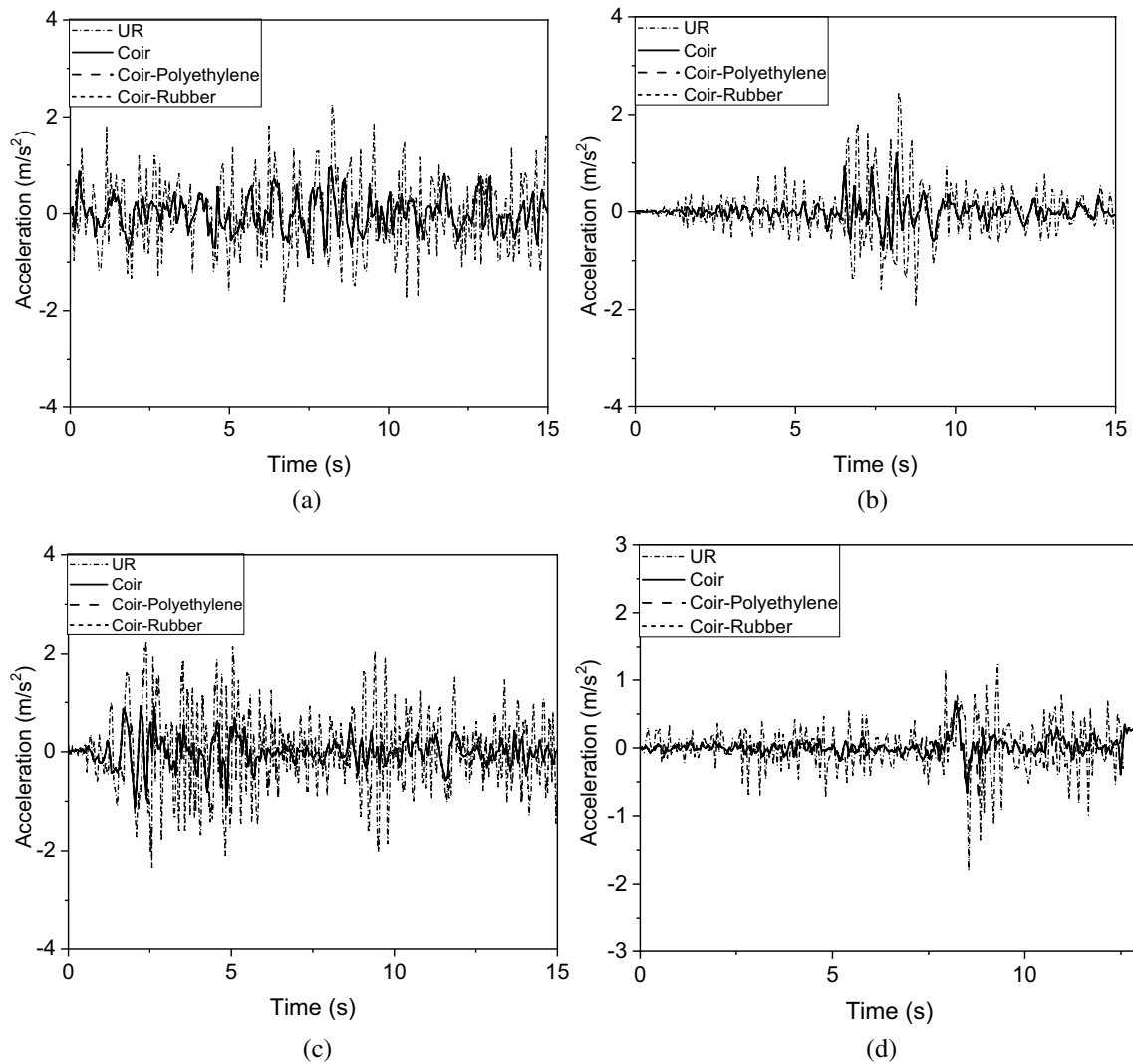


Fig. 11 Acceleration time history at the bottom of building for reinforced and unreinforced cases of soil under input motion; (a) EQ-1, (b) EQ-2, (c) EQ-3, (d) EQ-4

rubber material imparts additional isolation efficiency to the coir mat in reducing the seismic responses in the soil-structure system. And providing coir composite,

especially coir–polyethylene, gives long durability for the coir mat and better isolation efficiency in isolating seismic responses.

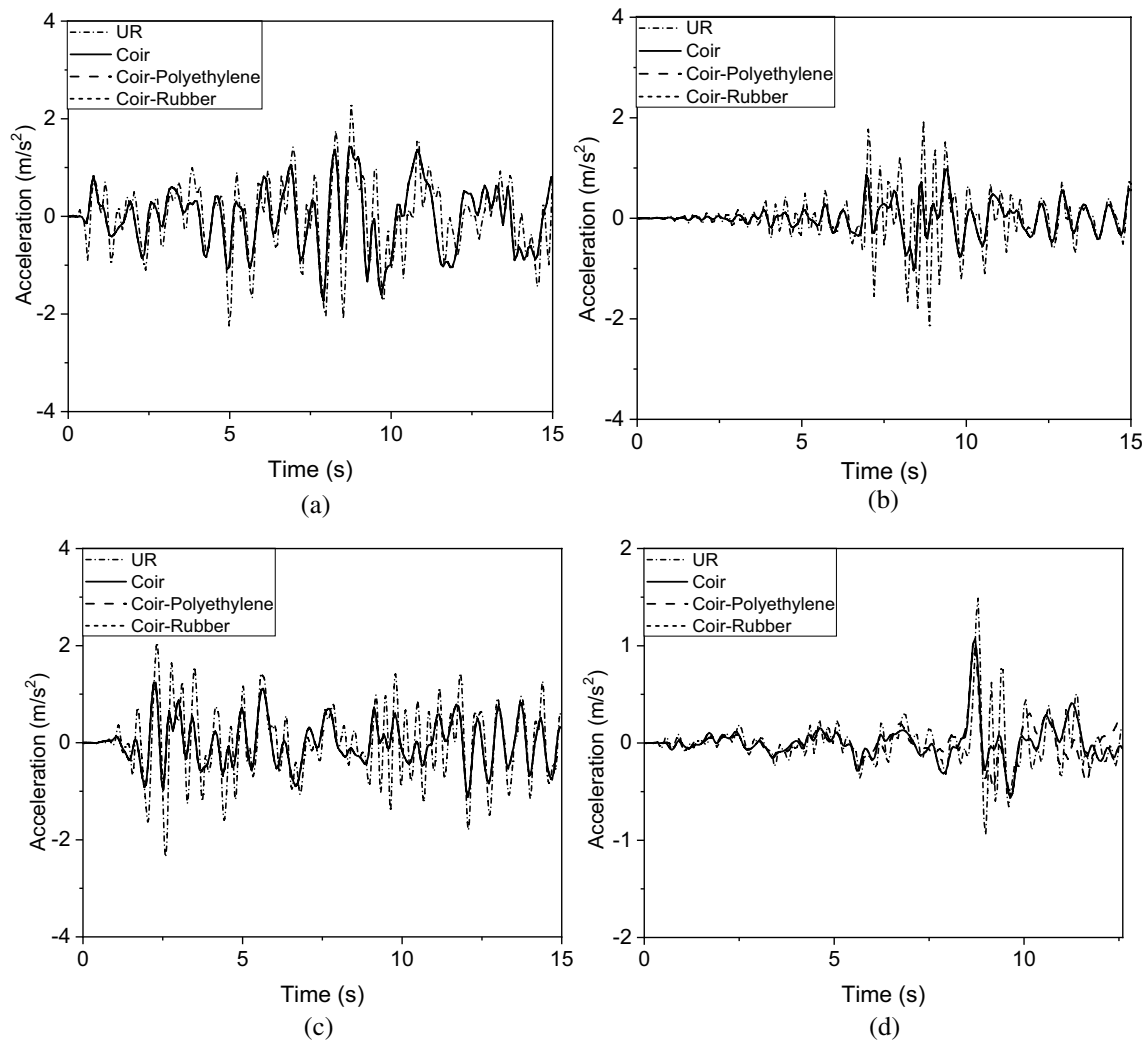


Fig. 12 Acceleration time history at the top of building for reinforced and unreinforced cases of soil under input motion; (a) EQ-1, (b) EQ-2, (c) EQ-3, (d) EQ-4

Author contributions All authors contributed to the study conception and design. Material preparation, data collection, and analysis were performed by SMV. The first draft of the manuscript was written by SMV. All authors commented on previous versions of the document. All authors have read and approved the final manuscript.

Data availability The datasets generated during and/or analyzed during the current research are available from the corresponding author on reasonable request.

Declarations

Conflict of interest On behalf of all authors, the corresponding author states that there is no conflict of interest.

References

1. Acacio AA, Kobayashi Y, Towhata I, Bautista RTIK (1977) Subsidence of building foundation resting upon liquefied subsoil case studies and assessment. *Chem Pharm Bull* 57:364–370
2. Yoshimi Y, Tokimatsu K (1977) Settlement of buildings on saturated sand during earthquakes. *Chem Pharm Bull* 57:364–370
3. Ishihara K, Acacio AATI (1994) Liquefaction-induced ground damage in Dagupan in the July 16, 1990 Luzon earthquake. *Chem Pharm Bull* 17:1460–1462
4. Liu L, Dobry R (1997) Seismic Response of Shallow Foundation on Liquefiable Sand. *J Geotech Geoenvironmental Eng* 123:557–567. [https://doi.org/10.1061/\(asce\)1090-0241\(1997\)123:6\(557\)](https://doi.org/10.1061/(asce)1090-0241(1997)123:6(557))
5. Lau K tak, Hung P yan, Zhu MH, Hui D (2018) Properties of natural fibre composites for structural engineering applications. *Compos Part B Eng* 136:222–233
6. Krishna Adhikari R, Keerthi Gowda BS (2017) Exploration of mechanical properties of banana/jute hybrid polyester composite. *Mater Today Proc* 4:7171–7176. <https://doi.org/10.1016/j.matpr.2017.07.043>

7. Leitão Borges J, Silva Cardoso A (2001) Structural behaviour and parametric study of reinforced embankments on soft clays. *Comput Geotech* 28:209–233. [https://doi.org/10.1016/S0266-352X\(00\)00021-5](https://doi.org/10.1016/S0266-352X(00)00021-5)
8. Borges JL, Cardoso AS (2002) Overall stability of geosynthetic-reinforced embankments on soft soils. *Geotext Geomembranes* 20:395–421. [https://doi.org/10.1016/S0266-1144\(02\)00014-6](https://doi.org/10.1016/S0266-1144(02)00014-6)
9. Rowe BRK (1984) Reinforced embankments: analysis and design. 110:231–246
10. Srilatha N, Latha GM, Puttappa CG (2016) Seismic response of soil slopes in shaking table tests: effect of type and quantity of reinforcement. *Int J Geosynth Gr Eng* 2:1–13. <https://doi.org/10.1007/s40891-016-0074-2>
11. Jha JN, Shukla SK (2015) Bearing Capacity and Settlement Characteristics of Sand Subgrades with Vertical Reinforcement Supporting a Square Footing. *Int J Geosynth Gr Eng* 1:1–13. <https://doi.org/10.1007/s40891-015-0018-2>
12. Nanda RP, Dutta S, Das A, Khan HA (2017) Geosynthetic Liner as Foundation Isolation for Seismic Protection. *Int J Geosynth Gr Eng* 3:0. <https://doi.org/10.1007/s40891-017-0098-2>
13. Kou Y, Shukla SK (2019) Analytical Investigation of Load Over Pipe Covered with Geosynthetic-Reinforced Sandy Soil. *Int J Geosynth Gr Eng* 5:0. <https://doi.org/10.1007/s40891-019-0156-z>
14. Borges JL (2004) Three-dimensional analysis of embankments on soft soils incorporating vertical drains by finite element method. *Comput Geotech* 31:665–676. <https://doi.org/10.1016/j.compgeo.2004.11.001>
15. Shen SL, Chai JC, Hong ZS, Cai FX (2005) Analysis of field performance of embankments on soft clay deposit with and without PVD-improvement. *Geotext Geomembranes* 23:463–485. <https://doi.org/10.1016/j.geotextmem.2005.05.002>
16. Al-Oqla FM, Sapuan SM, Anwar T et al (2015) Natural fibre reinforced conductive polymer composites as functional materials: A review. *Synth Met* 206:42–54. <https://doi.org/10.1016/j.synthmet.2015.04.014>
17. Sanjay MR, Madhu P, Jawaid M et al (2018) Characterization and properties of natural fibre polymer composites: A comprehensive review. *J Clean Prod* 172:566–581. <https://doi.org/10.1016/j.jclepro.2017.10.101>
18. Dicker MPM, Duckworth PF, Baker AB et al (2014) Green composites: A review of material attributes and complementary applications. *Compos Part A Appl Sci Manuf* 56:280–289. <https://doi.org/10.1016/j.compositesa.2013.10.014>
19. Westman M P, Field L S, Simmons K L LSG and KTA (2010) Natural Fibre Composites: A Review. *J Phycol* 35:806–814. <https://doi.org/10.1046/j.1529-8817.1999.3540806.x>
20. Chen J, Chouh N (2016) Compressive behaviour of flax FRP double tube confined coconut fibre reinforced concrete. *Constr Build Mater* 112:666–673. <https://doi.org/10.1016/j.conbuildmat.2016.02.120>
21. Scalici T, Fiore V, Valenza A (2016) Effect of plasma treatment on the properties of *Arundo Donax* L. leaf fibers and its bio-based epoxy composites: a preliminary study. *Compos Part B Eng* 94:167–175. <https://doi.org/10.1016/j.compositesb.2016.03.053>
22. Monte MC, Fuente E, Blanco A, Negro C (2009) Waste management from pulp and paper production in the European Union. *Waste Manag* 29:293–308. <https://doi.org/10.1016/j.wasman.2008.02.002>
23. Väisänen T, Haapala A, Lappalainen R, Tomppo L (2016) Utilization of agricultural and forest industry waste and residues in natural fibre-polymer composites: a review. *Waste Manag* 54:62–73. <https://doi.org/10.1016/j.wasman.2016.04.037>
24. A. D, Manaf SABA, S. Y, et al (2016) Low cost, high performance supercapacitor electrode using coconut wastes: eco-friendly approach. *J Energy Chem* 25:880–887 <https://doi.org/10.1016/j.jechem.2016.08.002>
25. Barkoula NM, Alcock B, Cabrera NO, Peijs T (2008) Flame-Retardancy Properties of Intumescent Ammonium Poly(Phosphate) and Mineral Filler Magnesium Hydroxide in Combination with Graphene. *Polym Polym Compos* 16:101–113. 10.1002/pc
26. Krishnaswamy NR, Thomas Isaac N (1995) Liquefaction analysis of saturated reinforced granular soils. *J Geotech Eng* 121:645–651. [https://doi.org/10.1061/\(ASCE\)0733-9410\(1995\)121:9\(645\)](https://doi.org/10.1061/(ASCE)0733-9410(1995)121:9(645))
27. Noorzad R, Fardad Amini P (2014) Liquefaction resistance of Babolsar sand reinforced with randomly distributed fibers under cyclic loading. *Soil Dyn Earthq Eng* 66:281–292. <https://doi.org/10.1016/j.soildyn.2014.07.011>
28. Maheshwari BK, Singh HP, Saran S (2012) Effects of reinforcement on liquefaction resistance of solani sand. *J Geotech Geoenvironmental Eng* 138:831–840. [https://doi.org/10.1061/\(asce\)gt.1943-5606.0000645](https://doi.org/10.1061/(asce)gt.1943-5606.0000645)
29. Ali M (2010) Coconut fibre - A versatile material and its applications in engineering. *2nd Int Conf Sustain Constr Mater Technol* 1441–1454
30. Munirah Abdullah N, Ahmad I (2012) Effect of chemical treatment on mechanical and water-sorption properties coconut fibre-unsaturated polyester from recycled PET. *ISRN Mater Sci* 2012:1–8. <https://doi.org/10.5402/2012/134683>
31. Tsang HH (2007) Seismic isolation for low-to-medium-rise buildings using granulated rubber-soil mixtures: numerical study Hing-Ho. *Pacific Conf Earthq Eng* 1–6. <https://doi.org/10.1002/eqe>
32. Zarnani S, Bathurst RJ (2005) Numerical investigation of geofam seismic buffers using FLAC. *Proc North Am Geosynth Soc (NAGS)/GRI19 Conf Las Vegas, Nev* 14–16
33. Tatlisoz N, Edil TB, Benson CH (1998) Interaction between reinforcing geosynthetics and soil-tire chip mixtures. *J Geotech Geoenvironmental Eng* 124:1109–1119. [https://doi.org/10.1061/\(asce\)1090-0241\(1998\)124:11\(1109\)](https://doi.org/10.1061/(asce)1090-0241(1998)124:11(1109))
34. Elragi AF (2006) Selected Engineering Properties and Applications of EPS Geofam. 39
35. Indraratna B, Ionescu D, Christie HD (1998) Shear behavior of railway ballast based on large-scale triaxial tests. *J Geotech Geoenvironmental Eng* 124:439–449. [https://doi.org/10.1061/\(asce\)1090-0241\(1998\)124:5\(439\)](https://doi.org/10.1061/(asce)1090-0241(1998)124:5(439))
36. Consoli NC, Montardo JP, Prietto PDM, Pasa GS (2002) Engineering behavior of a sand reinforced with plastic waste. *J Geotech Geoenvironmental Eng* 128:462–472. [https://doi.org/10.1061/\(asce\)1090-0241\(2002\)128:6\(462\)](https://doi.org/10.1061/(asce)1090-0241(2002)128:6(462))
37. Choudhary AK, Jha JN, Gill KS (2010) a Study on Cbr behavior of waste plastic strip reinforced soil. *Emirates J Eng Res* 15:51–57
38. Shao W, Cetin B, Li Y et al (2014) Experimental investigation of mechanical properties of sands reinforced with discrete randomly distributed fibre. *Geotech Geol Eng* 32:901–910. <https://doi.org/10.1007/s10706-014-9766-3>
39. Stark TD, Bartlett SF, Arellano D (2012) Expanded polystyrene (EPS) geofam applications and technical data. *EPS Ind Alliance* 1298:36
40. IS:2720 (Part 1): 1983 (1983) Methods of test for soils, Part 1: Preparation of dry soil samples for various tests. *Bur Indian Stand New Delhi Reaffirmed*:1–10
41. Nguyen TT, Indraratna B (2017) The permeability of natural fibre drains, capturing their micro-features. *Proc Inst Civ Eng Gr Improv* 170:123–136. <https://doi.org/10.1680/jgrim.16.00032>
42. Vries DVWM De (2009) the Mechanics of Foam. 3
43. Bledzki AK, Gassan J (1999) Composites reinforced with cellulose_Bledzki_1999.pdf. *Prog Polym Sci* 24:221–274
44. Bolarinwa OWA (2008) Mechanical property evaluation of coconut fibre. *BioResources* 7:923–932

45. ASTM D7180 Expanded Polystyrene Geofoam Applications & Technical Data Geofoam Applications & Technical Data
46. ASTM D6817 / D6817M-17 (2017) Standard Specification for Rigid Cellular Polystyrene Geofoam. ASTM Int 1–8. <https://doi.org/10.1520/D6817>
47. D5321 A (2019) Geosynthetic Interface Shear Testing. 1–59
48. Fischer-Cripps AC (2004) Materials data. Phys Companion. <https://doi.org/10.1887/0750309539/b1258b1>
49. Zhao Y, Ling X, Gong W et al (2020) Mechanical properties of fibre-reinforced soil under triaxial compression and parameter determination based on the duncan-chang model. Appl Sci 10:1–16. <https://doi.org/10.3390/app10249043>

Publisher's Note Springer Nature remains neutral with regard to jurisdictional claims in published maps and institutional affiliations.